microplastics

Article

Microplastic Deposits Prediction on Urban Sandy Beaches: Integrating Remote Sensing, GNSS Positioning, µ-Raman Spectroscopy, and Machine Learning Models

Anderson Targino da Silva Ferreira [1,2,3,*], Regina Célia de Oliveira [2], Eduardo Siegle [3], Maria Carolina Hernandez Ribeiro [4], Luciana Slomp Esteves [5], Maria Kuznetsova [1], Jessica Dipold [1], Anderson Zanardi de Freitas [1] and Niklaus Ursus Wetter [1,*]

1 Nuclear and Energy Research Institute, São Paulo 05508-000, Brazil; ma.kuznetsova88@gmail.com (M.K.); jessica.dipold@gmail.com (J.D.); azanardi@ipen.br (A.Z.d.F.)
2 Institute of Geosciences, State University of Campinas, Campinas 13083-855, Brazil; regina5@unicamp.br
3 Oceanographic Institute, University of São Paulo, São Paulo 05508-120, Brazil; esiegle@usp.br
4 School of Arts, Sciences and Humanities, University of São Paulo, São Paulo 03828-000, Brazil; maria.carolina.ribeiro@alumni.usp.br
5 Department of Life & Environmental Sciences, Bournemouth University, Poole BH12 5BB, UK; lucianasesteves@gmail.com
* Correspondence: andersontsferreira@gmail.com (A.T.d.S.F.); nuwetter@ipen.br (N.U.W.)

Abstract: This study focuses on the deposition of microplastics (MPs) on urban beaches along the central São Paulo coastline, utilizing advanced methodologies such as remote sensing, GNSS altimetric surveys, µ-Raman spectroscopy, and machine learning (ML) models. MP concentrations ranged from 6 to 35 MPs/m^2, with the highest densities observed near the Port of Santos, attributed to industrial and port activities. The predominant MP types identified were foams (48.7%), fragments (27.7%), and pellets (23.2%), while fibers were rare (0.4%). Beach slope and orientation were found to facilitate the concentration of MP deposition, particularly for foams and pellets. The study's ML models showed high predictive accuracy, with Random Forest and Gradient Boosting performing exceptionally well for specific MP categories (pellet, fragment, fiber, foam, and film). Polymer characterization revealed the prevalence of polyethylene, polypropylene, and polystyrene, reflecting sources such as disposable packaging and industrial raw materials. The findings emphasize the need for improved waste management and targeted urban beach cleanups, which currently fail to address smaller MPs effectively. This research highlights the critical role of combining in situ data with predictive models to understand MP dynamics in coastal environments. It provides actionable insights for mitigation strategies and contributes to global efforts aligned with the Sustainable Development Goals, particularly SDG 14, aimed at conserving marine ecosystems and reducing pollution.

Keywords: large microplastic; big data; altimetric position; laser application; multivariate statistical techniques

Academic Editor: Nicolas Kalogerakis

Received: 30 November 2024
Revised: 29 January 2025
Accepted: 27 February 2025
Published: 5 March 2025

Citation: Ferreira, A.T.d.S.; Oliveira, R.C.d.; Siegle, E.; Ribeiro, M.C.H.; Esteves, L.S.; Kuznetsova, M.; Dipold, J.; Freitas, A.Z.d.; Wetter, N.U. Microplastic Deposits Prediction on Urban Sandy Beaches: Integrating Remote Sensing, GNSS Positioning, µ-Raman Spectroscopy, and Machine Learning Models. *Microplastics* **2025**, *4*, 12. https://doi.org/10.3390/microplastics4010012

1. Introduction

Considered an emerging and persistent anthropogenic contaminant, microplastics (MPs) are also present as large particles, ranging from 1 to 5 mm [1], in various forms, such as pellets, foam, fragments, fibers, and films [2]. In urban environments, these particles enter ecosystems through rivers and drainage systems and flow towards the coast, where they are transported by coastal currents and storm events that enhance their accumulation [3–5].

Improper waste disposal, urban runoff, waste from leisure activities within these regions, and industrial activities are among the primary sources of MPs in coastal areas [4,6–8]. MPs are widely distributed on urban beaches, where concentrations are exceptionally high due to intense human activity (i.e., population pressure) and proximity to these pollution sources [9–11], with accumulation amplified by inadequate infrastructure for managing this pollutant, even with proper cleaning actions [12].

References [12–14] corroborate the aforementioned observation. Reference [14] highlights that the high occurrence of MPs on these beaches is primarily driven by urban stormwater, rivers, estuaries, and oceanic inputs. Similarly, ref. [15] noted that beaches with higher recreational value also exhibit elevated levels of MP contamination. Even those considered "contaminant-free", such as Blue Flag-certified beaches [16,17], appear not to be exempt from this pollutant [18]. Beyond coastal ecosystem health, the esthetics and leisure quality of beaches are also negatively impacted [19–21], harming tourism and economically devaluing these areas [22].

Mechanical abrasion and ultraviolet (UV) radiation accelerate the degradation and fragmentation of MPs [23,24], which may contribute to the release of greenhouse gases (GHG), primarily methane and ethylene [22,25]. Globally, research on MPs in urban beach environments primarily focuses on diagnosing abundance, contaminant load, and the surface characteristics of the material [25–30]. On Brazilian sandy beaches, these studies have primarily been quantitative [31]. Specifically, on the São Paulo coastline, recent studies have shown that the upper portions of the beach profile are more susceptible to deposition and accumulation of this pollutant, influenced mainly by geodesic, morphometric, and meteoceanographic factors [3,4,32].

Studies that use data from different sources help to identify possible hotspots and develop strategies to address plastic pollution in coastal regions [33]. Evaluations combining machine learning (ML) with hydrodynamic models have proven effective for predicting the distribution and deposition of MPs on sandy beaches, integrating large amounts of data and complex environmental variables such as ocean currents, winds, and human activities [34–38]. Furthermore, μ-Raman spectroscopy serves as a powerful tool for the rapid and precise identification of the polymeric characterization of deposited MP, such as polyethylene (PE), polypropylene (PP), polystyrene (PS) [39], and polyethylene terephthalate (PET), further enhancing knowledge about the behavior of this pollutant in these environments [3], such as in evaluating pollution sources, dispersion pathways, and the potential accumulation of MPs in the beach environment [40–42].

In this context, this study aims to understand the dynamics (i.e., concentration and distribution) of this material on urban beaches along the central São Paulo coastline, employing in situ surveys such as sediment collection, morphometric aspects (altitude, slope, and orientation of beach faces), orbital remote sensing images, and μ-Raman spectroscopy. We applied ML models to predict the deposition of MPs, advancing scientific knowledge about their presence and impact in urban coastal environments and providing precise information for managers and decision-makers. Regarding this purpose, this research also contributes to the United Nations' 2030 Agenda for Sustainable Development Goals (SDGs), particularly SDG 14, which aims to conserve and promote the sustainable use of oceans, seas, and marine resources [43].

2. Methodological Approach

The identification and characterization of sites susceptible to MP deposition involve four key steps: (1) determining beach face orientation and slope parameters derived from remote sensing imagery; (2) conducting fieldwork, including sediment collection and the measurement of beach morphometric parameters (orientation, slope, and altitude) using

Global Navigation Satellite System (GNSS) altimetry; (3) performing laboratory analysis (sieving and µ-Raman spectroscopy); and (4) applying machine learning (ML) models (Figure 1).

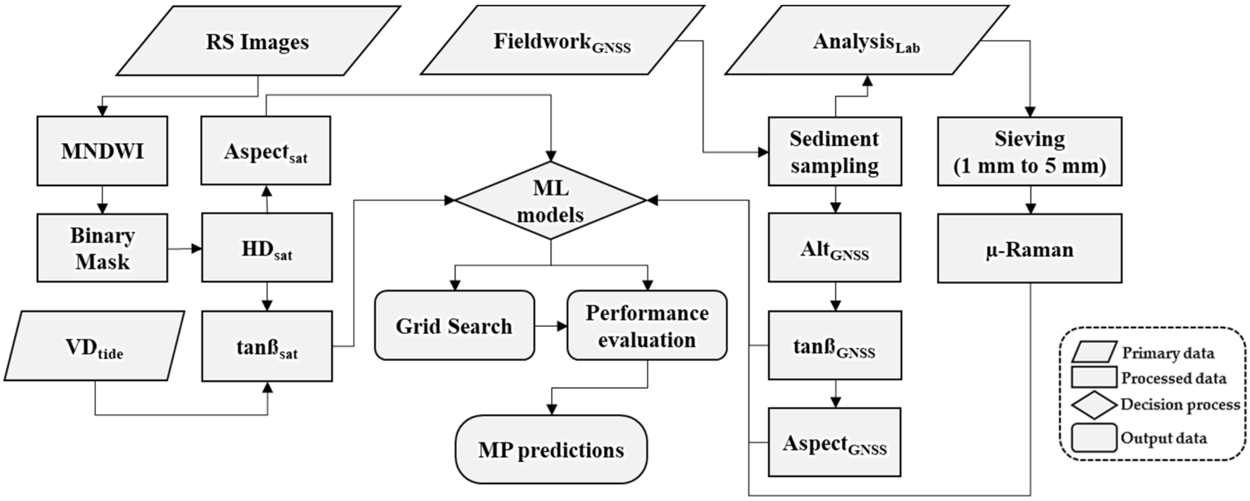

Figure 1. Flowchart of the steps in the methodology used in this research. RS: orbital remote sensing images; MNDWI: modified normalized difference water index; HD_{sat}: horizontal distance derived by satellite; VD_{tide}: vertical distance derived by tide; $\tan\beta_{sat}$: slope derived by satellite; GNSS: global navigation satellite system; Alt_{GNSS}: altitude derived by GNSS; $\tan\beta_{GNSS}$: slope derived by GNSS; µ-Raman: micro-Raman analysis; ML: machine learning models; and MP deposits: microplastic deposits.

2.1. Study Area

The central portion of the São Paulo coastline features sandy beaches, mangroves, resting vegetation (coastal vegetation found in sandy areas in Brazil), and estuarine systems, where natural processes and human activities shape its dynamics (Figure 2). Sedimentation and erosion, driven by longshore currents and longitudinal transport, redistribute sediments and debris along the coast [3,4,32,44]. East–northeast (E-NE) winds generate waves and, consequently, alongshore currents parallel to the shoreline, while atmospheric systems like the South Atlantic Tropical Anticyclone modify this dynamic, intensifying sediment transport and driving changes in beach morphology that affect the deposition and remobilization of MPs [3,4,32,44–47].

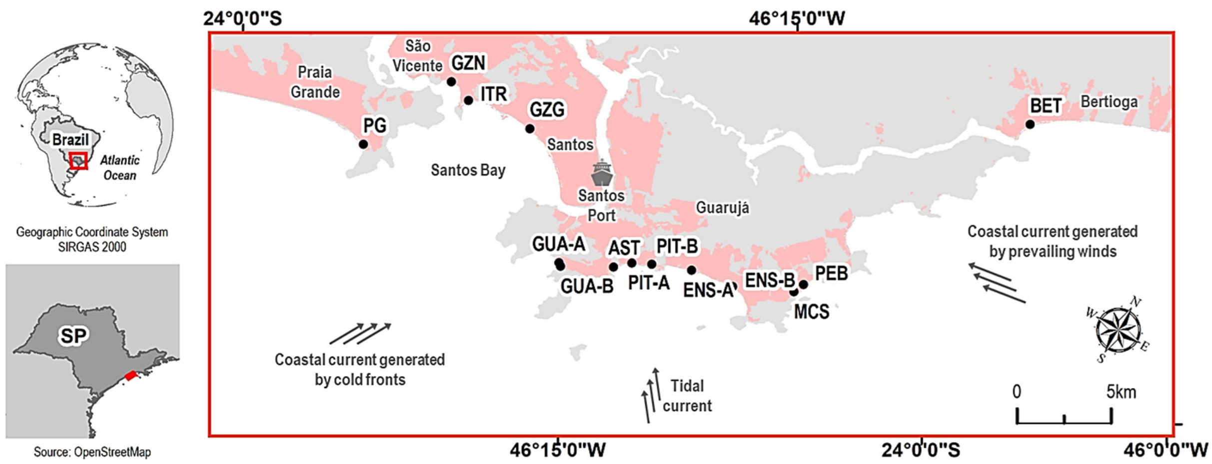

Figure 2. Sediment sampling sites and GNSS positioning locations. Urban areas are highlighted in red, with emphasis on the Port of Santos and the industrial region of Cubatão.

The proximity of urbanized areas, such as the Port of Santos and the industrial region of Cubatão, increases pressure on ecosystems, resulting in mangrove degradation, resting suppression, and the construction of artificial structures. These urban areas serve as significant sources of waste, including MPs from tourism and industrial and port activities, exacerbating environmental impacts in the region [3,4,48,49].

2.2. Remote Sensing Images

The beach face orientation ($Aspect_{sat}$) was determined based on the alignment of the transect relative to the geographic north [3,32,50]. The slope model (tanβsat in Equation (1)) was computed using the horizontal (HD_{sat}) and vertical (VD_{sat}) distances between the high and low tide shorelines, as identified from satellite imagery, along with the spring tide range [32]. For example, in the vicinity of the Port of Santos, the average spring tide range is 1.58 m, calculated using the mean sea level (MSL) reference from Imbituba/SC within the Brazilian Geodetic System (BGS) [4,32,51].

$$\tan\beta = \mathrm{atan}\ (VD/HD) \quad (1)$$

The HD_{sat} values were obtained from multispectral remote sensing (RS) data, integrating harmonized Landsat 8 and Sentinel-2 imagery (HLS) at a spatial resolution adjusted to 30 m for 2019 and 2021. This methodology allows for up to seven satellite observations per month for the same area [32,52]. Median HLS images were collected during synchronous satellite passes (~10:30 A.M.) aligned with high and low spring tide phases, using tidal predictions from the WXTIDE32 software v. 4.7 [53]. Consequently, two datasets—High Tide (HT) and Low Tide (LT)—were developed, each based on the median of 26 HT and 27 LT images. The beach slope data derived from satellite imagery facilitated a rapid empirical assessment of the beach slope, and were classified into three categories: steep ($\tan\beta > 0.12$), intermediate ($0.05 < \tan\beta < 0.12$), and gentle ($\tan\beta < 0.05$) [3,32,54,55].

2.3. Fieldwork Samples and Laboratory Analysis

Fieldwork took place from April to September 2023, examining ten beach profiles with varying slopes and orientations aligned with the spring tide period. During this time, cold fronts generated waves up to 4 m high, arriving predominantly from the south and southeast quadrants [47]. These conditions significantly influenced sediment dynamics, reshaping beach morphology and affecting the deposition and remobilization of microplastics [3,4,32]. The selected beach profiles represented both urbanized and non-urbanized stretches of São Paulo's coastline. Sediment samples and morphometric data were systematically collected along these profiles, as outlined in Table 1 and Figure 2.

Table 1. Standardized qualitative data based on the total microplastics (MP/m^2).

Ranking	Qualitative Data
0.80–1.00	Very High (VH)
0.60–0.79	High (H)
0.40–0.59	Moderate (M)
0.20–0.39	Low (L)
0.00–0.19	Very Low (VL)

Sampling locations within each profile were chosen based on environmental factors affecting debris distribution on sandy beaches, such as strandline elevations linked to water levels [4]. At each sampling point, approximately 1500 g of sediment was collected from the highest storm surge strandline (P1) [3]. These samples were then homogenized and divided into 500 g portions for consistency and potential replicate analyses. The surface sediment layer (~2 cm deep) was sampled over a 1 m^2 area (Figure 3) at each of the 40 points, leading to the identification of 272 microplastic particles between 1 and 5 mm in size [1,3].

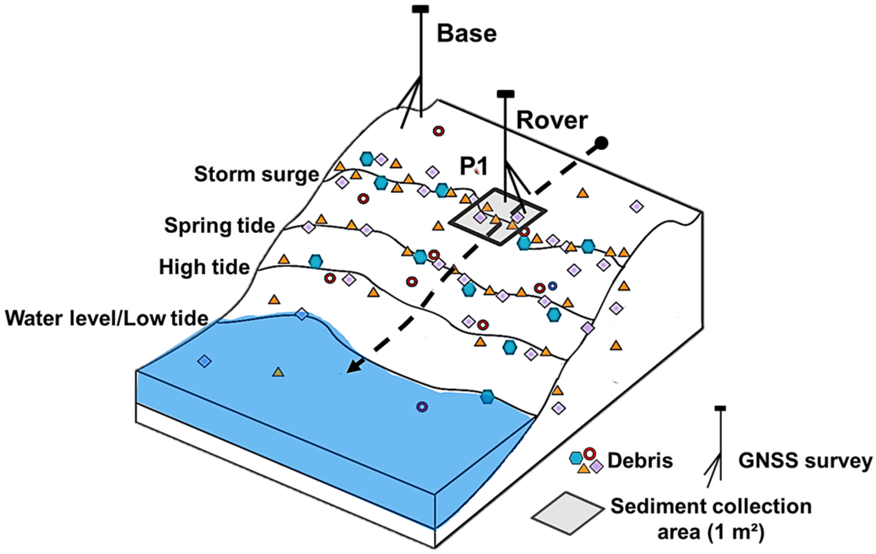

Figure 3. Beach sampling point (P1), modified from [1]. Examples of GNSS base, rover surveys, and area (1 m^2) of superficial sediment collection.

The in situ morphometric parameters ($Aspect_{GNSS}$, beach slope—$\tan\beta_{GNSS}$, and $Altitude_{GNSS}$) were obtained via a process similar to that described in Section 2.2. The orientation of the beach face ($Aspect_{sat}$) was established based on the direction of the transect relative to geographic north, and $\tan\beta_{GNSS}$, derived by VD and HD, are the vertical and horizontal distances (VD_{GNSS} and HD_{GNSS}) between sampling points P1 and water level/low tide, respectively (Equation (1); Figure 3). The slope can be used as a proxy of the beach's morphodynamic stage [54]. Orthometric altitudes (H_i) were determined using the GNSS positioning obtained using the fast static relative GNSS surveying method, referencing the mean sea level at Imbituba-SC, calculated based on the SIRGAS2000 ellipsoid (h_i) and the MAPGEO2015 geoid height model (N_i) [3,4,56,57] (Equation (2)).

$$H_i = h_i - N_i \tag{2}$$

Approximately 60% of the samples are characterized using μ-Raman spectroscopy [58] with the labRAM HR Evolution spectrometer, which operates with a long-range objective lens featuring a numerical aperture (NA = 0.55) and lasers of various wavelengths (473 nm, 532 nm, 633 nm, 785 nm, and 1064 nm), covering a spectral range of 200 cm^{-1} to 3200 cm^{-1} for hydrocarbon detection [3,59–61]. To maximize spectrum quality, measurement parameters such as integration time, the number of accumulations, and slit diameter are continuously adjusted. Noise filtering is applied to the baseline using MATLAB® v. 23.2. The filtered spectra are then compared against a database in the KnowItAll® v. 2024 artificial intelligence software to identify polymer types [3,60].

2.4. Machine Learning Models

The calibration between satellite-estimated variables ($\tan\beta_{sat}$ and $Aspect_{sat}$) and in situ, GNSS measurements ($\tan\beta_{GNSS}$ and $Aspect_{GNSS}$) applies the Random Forest model [62] and performance indicators such as the coefficient of determination (R^2), Mean Absolute Error (MAE), and Root Mean Squared Error (RMSE) to ensure accuracy [32]. To predict MP deposition (MP/m^2) on sandy beaches, machine learning (ML) algorithms are applied, using $\tan\beta_{GNSS}$ and $Aspect_{GNSS}$ as predictor variables. Due to the limited number of samples, the dataset (14 profiles) is randomly expanded by up to 120%. From this expanded dataset, 70% is allocated for training and 30% for validation, minimizing overfitting and underfitting [63,64].

The models applied in this stage include Random Forest (RF) [62], Gradient Boosting (GB) [65], Lasso and Ridge Regression [66,67], Support Vector Regression (SVR) [68,69], and Partial Least Squares Regression (PLS) [70]. Hyperparameters are optimized using Grid Search [71] and evaluated using metrics such as R^2, MAE, RMSE, Akaike Information Criterion (AIC), and Bayesian Information Criterion (BIC), along with overfitting and underfitting indicators [72–74]. SHapley Additive exPlanations (SHAP) analysis assesses the influence of independent variables on predictions, aiding in the selection of the most effective models [75].

Given the quantitative nature of the data resulting from the predictive models for beach face slope (tanβ) and orientation (Aspect), as well as MP deposition (MP/m^2), these are transformed into qualitative variables for the application of the exploratory multivariate Correspondence Analysis (CA) technique. This technique examines associations between the variables of interest using the chi-square test (X^2; p-value < 0.05). Adjusted standardized residuals (ASR) verify significant dependency relationships between each variable based on the critical reference value (+1.96 $\leq$ good ASR) of the standard normal curve at the 5% significance level [63,76,77]. Thus, tanβ values are classified as steeper, and intermediate, sloping, and Aspect values are categorized as N, NE, E, SE, S, SW, W, and NW, as described in Section 2.2. [32,50,54,55]. The results of the MP deposition model (pellets, foam, fragments, fiber, and film) (MP/m^2) are standardized (Equation (3)) and transformed into a Likert scale (Table 1). All statistical analyses use the Python programming language via the Anaconda/Spyder software v. 5.4.3, while geographic distribution is processed with ArcGIS Pro software v. 3.4.

$$Standardization = \frac{(observed\ value - minimum\ value)}{(maximum\ value - minimum\ value)} \tag{3}$$

3. Results

3.1. Morphometric Parameters and In Situ Microplastic Distribution

Table 2 summarizes the morphometric characteristics of altitude (Alt), slope (tanβ), Aspect, and the distribution of different microplastic categories per square meter (MP/m^2) collected in situ: pellets, fragments, fibers, foam, and films. Environmental characteristics, such as slope (tanβ) and Aspect, exhibit considerable variation among beaches. Slopes like GUA-A (tanβ = 0.157) tend to show higher concentrations of foam particles, suggesting that topography influences MP retention. Conversely, beaches with lower slopes, such as GNZ (tanβ = 0.004), exhibit less MPs. Among MP types, foam represents the highest proportion (48.7%), followed by fragments (27.7%) and pellets (23.2%). Fibers account for a minimal fraction (0.4%), and no films were recorded. The site with the highest MP/m^2 density is MCS-A beach, with 35 MP/m^2, followed by PG and BET, each with 28 MP/m^2 (Figure 2, Table 2).

Table 2. Altitude (Alt), slope (tanβ), Aspect, and distribution of different and total microplastic categories (MP/m^2).

COD	Alt	tanβ	Aspect	Pellet	Fragment	Fiber	Foam	Film	MP/m^2
BET	2.31	0.017	136	1	3	1	23	0	28
PEB-A	2.41	0.047	151	2	5	0	6	0	13
MCS-A	2.13	0.029	128	9	14	0	12	0	35
ENS-B	3.22	0.086	183	2	2	0	3	0	7

Table 2. *Cont.*

COD	Alt	tanβ	Aspect	Pellet	Fragment	Fiber	Foam	Film	MP/m^2
ENS-A	2.45	0.036	168	1	0	0	1	0	2
PIT-B	2.34	0.027	201	7	10	0	6	0	23
PIT-A	2.32	0.054	151	4	1	0	2	0	7
AST-A	2.57	0.075	112	1	0	0	5	0	6
GUA-B	2.45	0.05	224	5	0	0	11	0	16
GUA-A	2.41	0.157	217	1	2	0	15	0	18
GNZ	2.39	0.004	191	10	5	0	0	0	15
ITR	4.14	0.023	128	0	5	0	12	0	17
GZN	1.16	0.008	165	0	8	0	1	0	9
PG	1.47	0.014	213	9	7	0	12	0	28
Total				52	62	1	109	0	224
%				23.2	27.7	0.4	48.7	0	100

3.2. Model Calibration and Validation Metrics

The calibration of morphometric data between tanβ$_{GNSS}$ (in situ) and tanβ$_{sat}$ demonstrated strong performance using the Random Forest (RF) model, achieving a coefficient of determination (R^2) of 0.784, indicating that the model explained 78% of the variability in satellite-estimated slope. Error metrics confirmed the predictions' closeness to the actual values, with an MAE of 0.006 and an RMSE of 0.008. For the variable Aspect$_{sat}$, the model showed even better performance, with an R^2 of 0.848, explaining 85% of the variability, and MAE and RMSE values of 8.978 and 11.882, respectively, reaffirming RF's ability to capture relationships between morphometric variables in the training set.

In analyzing metrics related to MP categories (pellets, fragments, fibers, foams, and total MP/m^2), results varied depending on the microplastic type. For pellets, the SVR model achieved an R^2 of 0.596, MAE of 1.150, and RMSE of 1.695, classified as "Good Fit" for balancing simplicity and accuracy, with an AIC of 39.940 and BIC of 49.109. For fragments, the Gradient Boosting (GB) model stood out, with an R^2 of 0.904, MAE of 0.366, and RMSE of 1.051, demonstrating its robustness in predicting the variability of this MP type. For fibers, the RF model performed best, with an R^2 of 0.975, MAE of 0.023, and RMSE of 0.049, as well as negative AIC (−78.950) and BIC (−61.950) values, indicating high efficiency and model fit (Table 3).

Table 3. Performance metrics of machine learning models for predicting MP deposition.

MP	Model	R^2	MAE	RMSE	AIC	BIC	Overfit/Underfit
Pellet	SVR	0.596	1.150	1.695	39.940	49.106	Good Fit
Fragment	GB	0.904	0.366	1.052	43.719	61.217	Good Fit
Fiber	RF	0.975	0.023	0.049	−78.950	−61.950	Good Fit
Foam	RF	0.994	0.384	0.574	17.110	32.108	Good Fit
Film	Null	Null	Null	Null	Null	Null	Null
Total MP/m^2	GB	0.942	0.703	2.037	66.193	83.690	Good Fit

For foams, the RF model achieved an R^2 of 0.994, MAE of 0.384, and RMSE of 0.574, confirming its exceptional performance for this category. Films were excluded due to their absence. For total MP/m^2, the GB model showed significant performance, with an R^2 of 0.942, MAE of 0.703, and RMSE of 2.037, along with acceptable AIC and BIC values, demonstrating its robustness for integrated MP predictions (Table 3).

Figure 4a from the SVR model applied to pellets shows that tanβ has a more significant negative impact, with more dispersed values than Aspect, which contributes values close to zero. This analysis highlights tanβ as a key variable in the model, while Aspect plays a secondary but still relevant role. Figure 4b from the GB model for fragments shows that tanβ has a predominantly negative impact, while Aspect contributes more variably, with values near zero. The dispersion of points suggests differences in variable behavior under specific scenarios, with high values (in red) contributing more neutrally or positively. The horizontal axis reflects relative importance, while the colors indicate the attribute's intensity within the model's prediction context. The plot in Figure 4c examines the impact of variables in the RF model for fibers. Tanβ exerts minimal influence, with SHAP values near zero, indicating low predictive importance. Aspect shows slightly higher impacts in some cases, but remains modest. The absence of extreme SHAP values suggests that both variables play complementary but limited roles in the model. The color distribution reinforces the low variability of attributes within this dataset.

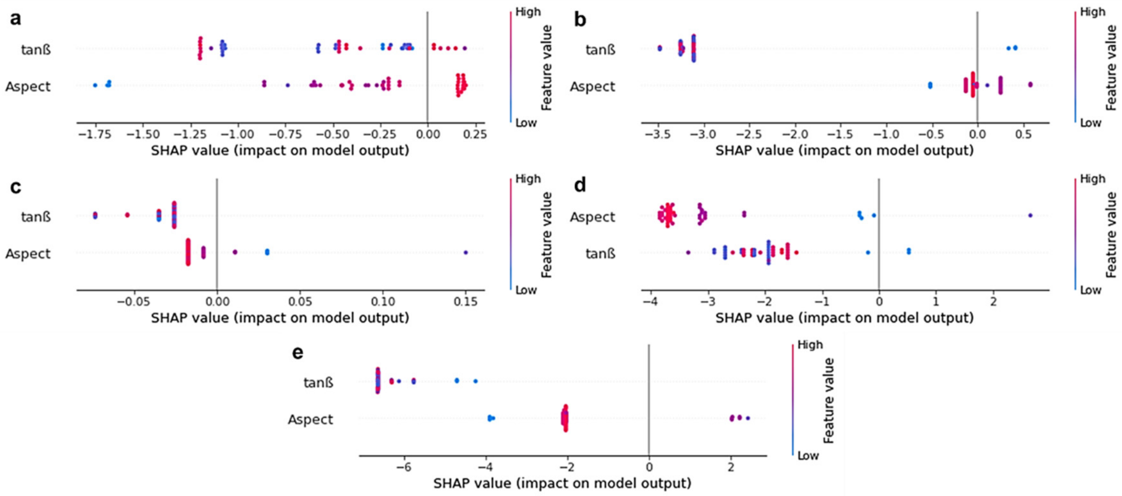

Figure 4. SHAP analysis of variable contributions for predicting microplastic deposition using multiple machine learning models: (**a**) SVR—Support Vector Regression for pellets; (**b**) GB—Gradient Boosting for fragments; (**c**) RF—Random Forest for fibers; (**d**) RF—Random Forest for foams; and (**e**) GB—Gradient Boosting for total MP. The intensity of each variable is represented by the color scale, ranging from blue (low values) to red (high values), indicating the magnitude of the feature's influence.

In Figure 4d, the RF model applied to foams reveals that Aspect has greater relevance, with broadly negative SHAP values, indicating its significant impact on predictions for this MP type. Tanβ also shows negative values, but with less dispersion. The graph further observes a strong correlation between Aspect and model outcomes. The color separation illustrates how high or low values influence predictions, with red generally associated with significant negative contributions. Figure 4e from the GB model applied to total MP demonstrates that tanβ has the most critical impact, with broadly negative SHAP values indicating an inverse correlation. Aspect also shows relevance, albeit to a lesser extent, with contributions ranging from negative to neutral. The varying colors of the points reflect the intensity of variables relative to predictions, highlighting how attributes independently influence the model's decision-making process.

3.3. Morphometric Parameters and Microplastic Distribution Models

Table 4 presents data on the predicted slope (tanβ) and Aspect of the beaches in Praia Grande (PG), São Vicente (SVS), Guarujá (GUA), and Bertioga (BER). The tanβ variable indicates that the beaches tend toward an intermediate morphodynamic state, with average slopes ranging from 0.059 in GUA to 0.064 in PG. The maximum slope observed was 0.071 across multiple beaches, supporting an intermediate morphodynamic pattern. The lowest slope variability was recorded in GUA (standard deviation, SD = 0.006), while the highest was observed in PG and BER (SD = 0.008).

Table 4. Statistical summary of the models: slope (tanβ) and direction of the beach face (Aspect).

Var.	Beach	N	Min	Max	Sum	Mean	SD
tanβ	PG	9	0.047	0.071	-	0.064	0.008
	SVS	14	0.055	0.071	-	0.063	0.007
	GUA	17	0.047	0.068	-	0.059	0.006
	BER	6	0.048	0.071	-	0.060	0.008
Aspect	PG	9	151	184	-	165	12
	SVS	14	151	184	-	171	13
	GUA	17	150	184	-	169	13
	BER	6	108	150	-	120	16

In the same table, average beach face orientations ranged from 120° in BER to 171° in SVS, reaching up to 184° in the southern central beaches of the study area (GUA, SVS, and PG), indicating that these beach faces are predominantly oriented toward the SSE quadrant. BER exhibited the highest variation (SD = 16), while PG had the lowest dispersion (SD = 12). The maps in Figure 5 corroborate Table 4, indicating the intermediate tendency of these beaches, with no steeper beaches observed and some sloping beaches identified in southern PG, northern GUA, and the central portion of BER. Similarly, beach face orientations vary along this stretch of the São Paulo coastline, with predominant SSE directions in PG, SVS, and GUA and a variation toward ESE in BER.

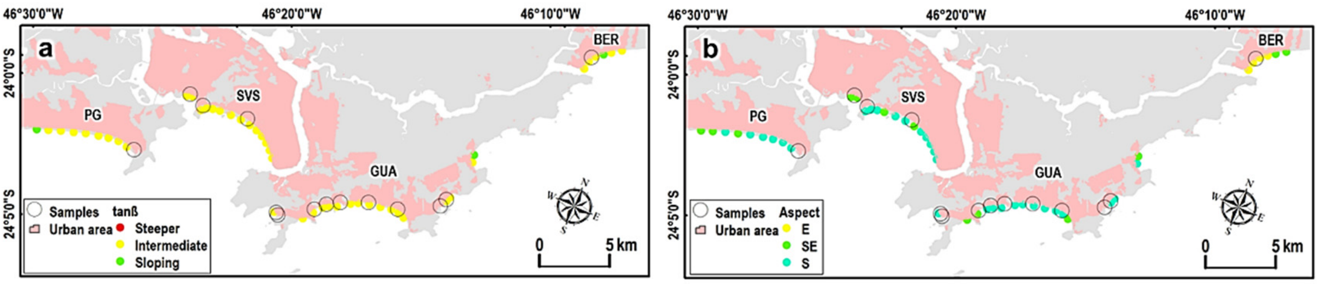

Figure 5. GNSS sediment samples and transect models: (**a**) beach slope (tanβ); (**b**) beach face direction (Aspect).

The Shapiro–Wilk test indicated that the all the different types of polymers do not fit the assumptions of parametric tests (p-value < 0.05), while the number of polymers found on the beaches (PG, SVS, GUA, and BER) is a dataset suitable for parametric testing (p-value > 0.05). In this context, the Kruskal–Wallis test for equal medians of polymer concentrations shows $X^2 = 76$ and p-value = 1.279×10^{-18}, indicating a significant difference between sample medians. The same Shapiro–Wilk test was applied. Furthermore, the t-test demonstrated a significant difference in the quantities of these polymers across the different beaches (p-value = 0.02549) [78].

Table 5 indicates that pellets were the models' most frequent type of MP, followed by foams and fragments, while fibers were the least frequent. Predictive models for pellets showed uniformity across the beaches PG, SVS, and GUA, with an average of 3 MP/m^2 (SD = 0), while BER had a lower average (2 MP/m^2) and greater variability (SD = 1). For foams, PG and BER exhibited the highest average values (3 and 5 MP/m^2, respectively), with greater variation in BER (SD = 2). SVS and GUA predicted lower average values

(2 MP/m^2), with low variability. For fragments, all beaches predicted an average of 1 MP/m^2, except BER, which showed greater variation (SD = 2), reflecting maximum values of 4 MP/m^2. Fibers were not predicted in PG, SVS, and GUA, while BER predicted an isolated case. The same table also shows homogeneity in the total MP predictions for PG, SVS, and GUA, with averages ranging from 7 to 8 MP/m^2 (SD $\leq$ 2), while BER displayed greater variability (SD = 3) and a wider range between the minimum and maximum values (6 and 12 MP/m^2). Table 5 highlights the predominance of pellets and foams across all beaches, with pellets being the most common category (135), followed by foams (127). Fragments accounted for 48, while fibers were nearly absent (1 MP). The total cumulative count for all categories was 349 MP.

Table 5. Statistical summary of the models of different concentrations of microplastic categories by beach (MP/m^2).

Var.	Beach	N	Min	Max	Sum	Mean	SD	Total
Pellet	PG	9	3	4	28	3	0	135
	SVS	14	3	4	42	3	0	
	GUA	17	3	4	50	3	0	
	BER	6	2	4	15	2	1	
Foam	PG	9	2	6	24	3	1	127
	SVS	14	2	3	32	2	0	
	GUA	17	2	6	40	2	1	
	BER	6	3	8	31	5	2	
Fragment	PG	9	1	5	12	1	1	48
	SVS	14	1	1	12	1	0	
	GUA	17	1	5	18	1	1	
	BER	6	0	4	6	1	2	
Fiber	PG	9	0	0	0	0	0	1
	SVS	14	0	0	0	0	0	
	GUA	17	0	0	0	0	0	
	BER	6	0	1	0	0	0	
Total MP	PG	9	7	13	69	8	2	349
	SVS	14	7	12	102	7	1	
	GUA	17	7	13	129	8	2	
	BER	6	6	12	49	8	3	

Spatial distribution prediction maps for MPs (Figure 6) support the abovementioned findings. Pellets (Figure 6a) showed the highest concentrations in PG and SVS (3–4 MP/m^2), intermediate values in GUA, and the lowest in BER. Foams (Figure 6b) had the highest concentrations in BER (6–8 MP/m^2), intermediate values in PG (4–6 MP/m^2), and the lowest in SVS and GUA (2–3 MP/m^2). Fragments (Figure 6c) revealed greater spatial heterogeneity, with the highest concentrations (5–6 MP/m^2) in specific areas of GUA and BER, while PG and SVS exhibited more moderate values (2–4 MP/m^2). Fibers (Figure 6d) were the least predicted MP, absent in PG, SVS, and GUA, and occurring only in BER (1 MP/m^2). Figure 6e, showing the total predicted MP accumulation, highlights PG and BER as the beaches with the highest concentrations (12–13 MP/m^2), followed by SVS and GUA, which showed moderate values (8–11 MP/m^2).

The X^2 test analyses indicate statistically significant associations between the categorical variables analyzed. The tanβ variable shows significant associations with pellets (p-value = 8.7135×10^{-5}), foams (p-value = 3.1183×10^{-8}), fragments (p-value = 2.5028×10^{-8}), and total MP (p-value = 2.2597×10^{-5}), highlighting relevant relationships between these variables. However, there is insufficient statistical evidence for a significant association between tanβ and fibers (p-value = 0.0750), though this value is close to the significance threshold of 0.05, suggesting a potential marginal relationship. The Aspect variable demonstrates a statistically significant association only with pellets (p-value = 1.0860×10^{-11}), indicating a strong relationship between these variables. For other variables, such as foams (p-value = 0.5645), fragments (p-value = 0.3904), fibers (p-value = 0.7411), and total MP (p-value = 0.3041), the p-values do not indicate significant associations, showing that Aspect has limited impact except for pellets.

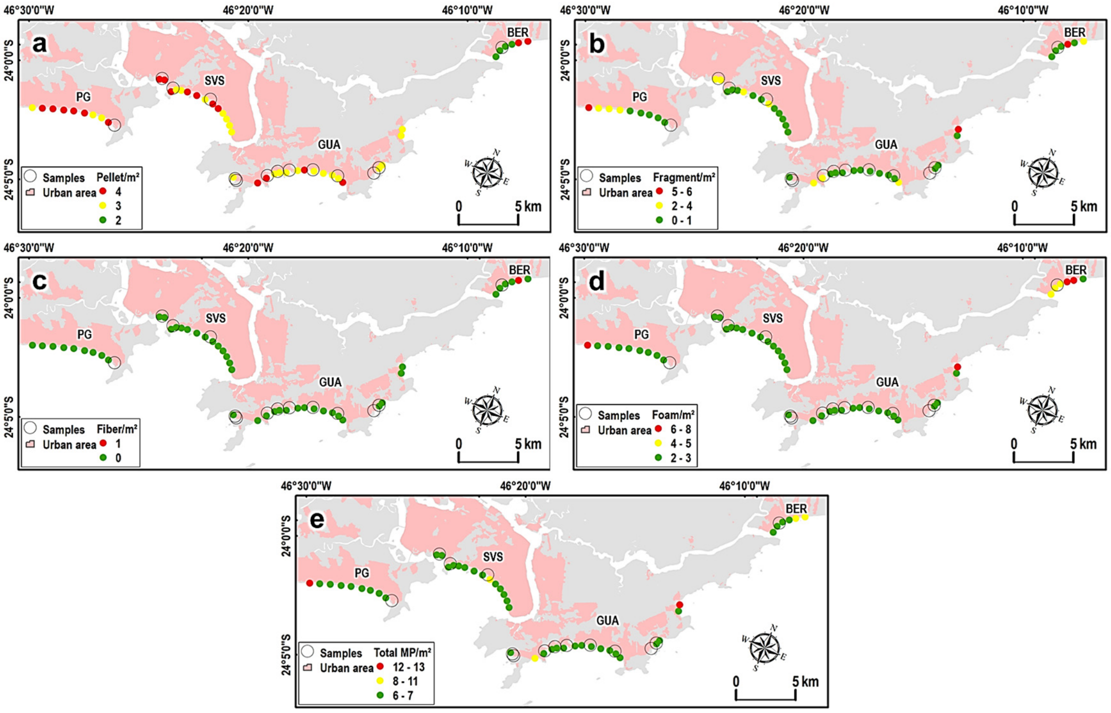

Figure 6. Modeled points and GNSS sediment sample points: (**a**) pellet, (**b**) foam, (**c**) fragment, (**d**) fiber, and (**e**) total MP (m^2).

The same X^2 test showed significant associations between different beaches (variable beach) and the categorical variables, mainly pellets, foams, fragments, and total MP. The strongest association was observed with pellets, with a p-value of 1.7431×10^{-12}, indicating a highly significant relationship. Additionally, significant associations were found between beaches and foams (p-value = 9.1400×10^{-5}) and fragments (p-value = 0.0042), suggesting relevant patterns of association for these categories. However, no significant associations were found for fibers, indicating insufficient evidence to establish a consistent relationship between these variables (p-value = 0.2404). Conversely, the analysis between the beach and total MP revealed a p-value of 6.9000e−06, indicating a highly significant association and reinforcing the relevance of this variable in explaining observed differences across beach categories.

Figure 7 illustrates the perceptual map of adjusted standardized residuals (ASR) for dependency relationships in the modeled points for PG, GUA, SVS, and BER, showing the different concentrations of pellets, foams, fragments, and total MP. Figure 7a demonstrates that VH (very high), H (high), M (medium), and VL (very low) concentrations of pellets are strongly associated with the modeled points in PG, GUA, SVS, and BER. VH, H, and M concentrations of foams are also related to PG (Figure 7b), as are VH concentrations of fragments (Figure 7c) and total MP (Figure 7d), which are strongly associated with the modeled points in PG. Fibers did not exhibit significant dependency relationships for any of the beaches.

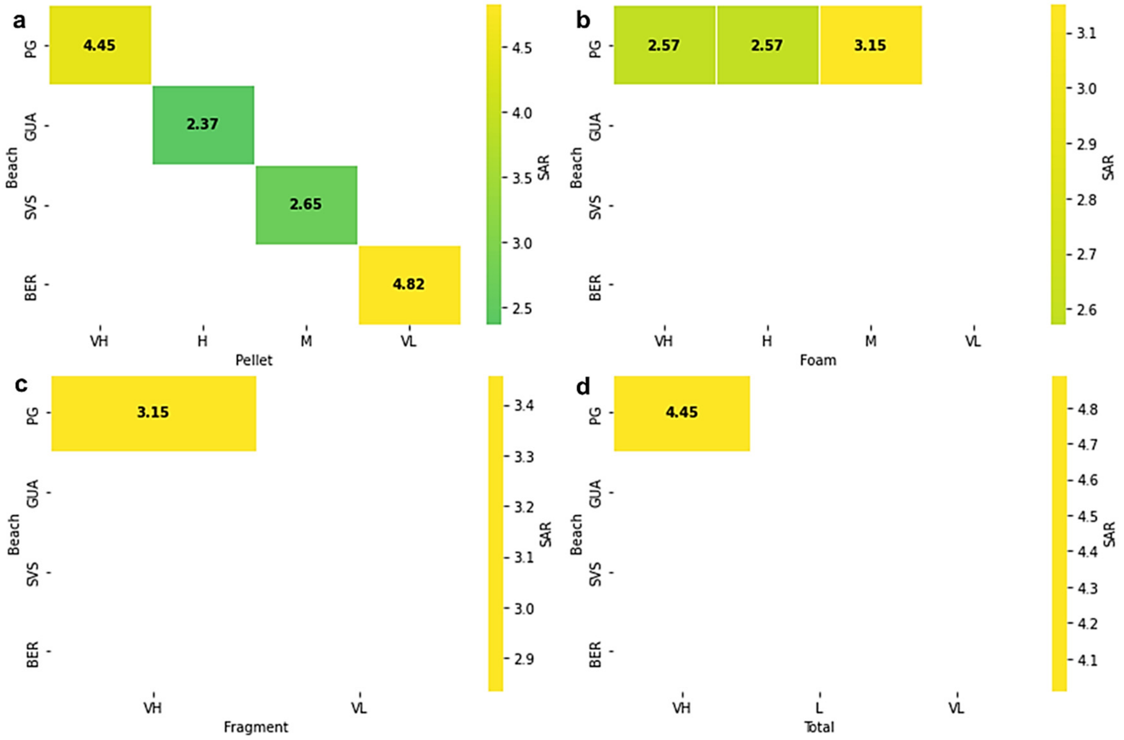

Figure 7. Perceptual maps showing the standardized adjusted residual (ASR) values between the microplastic deposition models: (**a**) pellet, (**b**) foam, (**c**) fragment, and (**d**) total MP (m^2) in relation to beaches' modeled points (PG, SVS, GUA, and BER). The colored cells indicate significant relationships between variables (+1.96 $\leq$ good SAR). VL (very low), L (low), M (medium), H (high), and VH (very high) represent the different levels of MP/m^2 deposition by CA.

3.4. Polymeric Characterization

The μ-Raman spectra of MP particles classified as pellets, foams, fragments, and fibers identify their chemical and physical characteristics. Pellets, frequently observed, appear in various shapes, such as spherical, disk-like, or cylindrical, with diverse colors and compositions. μ-Raman analysis reveals that high-density polyethylene (HDPE), with a density of 0.93–0.97 g/cm^3 and bands at 1.113 cm^{-1} and 1.412 cm^{-1}, is the most common (Figure 8a). Low-density polyethylene (LDPE), with a density of 0.91–0.93 g/cm^3 and bands at 1.061 cm^{-1}, 1.130 cm^{-1}, and 1.447 cm^{-1} (Figure 8b), is another frequently identified material. Polypropylene (PP), with a density of 0.89–0.92 g/cm^3 and bands at 809 cm^{-1}, 841 cm^{-1}, and 973 cm^{-1}, is the third most prevalent compound (Figure 8c). Polystyrene (PS), with a density of 1.05–1.15 g/cm^3 and bands at 620 cm^{-1} and 1.003 cm^{-1} (Figure 8d), ranks fourth.

Foams primarily comprise expanded polystyrene (EPS) or extruded polystyrene (XPS), with densities of 0.015–0.03 g/cm^3 and 0.03–0.06 g/cm^3, respectively. μ-Raman spectra reveal characteristic bands at 620 cm^{-1}, 1.003 cm^{-1}, and 1.609 cm^{-1} (Figure 8d), typical of the aromatic composition (C8H8)n. Fragments display Raman bands typical of polyethylene (PE—Figure 8a,b), polypropylene (PP—Figure 8c), and polystyrene (PS—Figure 8d), confirming compositions of (C2H4)n, (C3H6)n, and (C8H8)n. The density of these fragments varies according to the polymer; PE and PP (<1 g/cm^3) float in water, while PS (>1 g/cm^3) tends to deposit in sediments [23]. The varying colors observed indicate synthetic pigments (dyes) or environmental alterations [79]. Fibers, the least frequent, include polyamide (PA, nylon) and polyethylene terephthalate (PET), with bands at 1.132 cm^{-1} and 1.638 cm^{-1} (PA), and 1.000 cm^{-1} and 1.730 cm^{-1} (PET), and densities ranging from 1.14 to 1.38 g/cm^3 (Figure 8b).

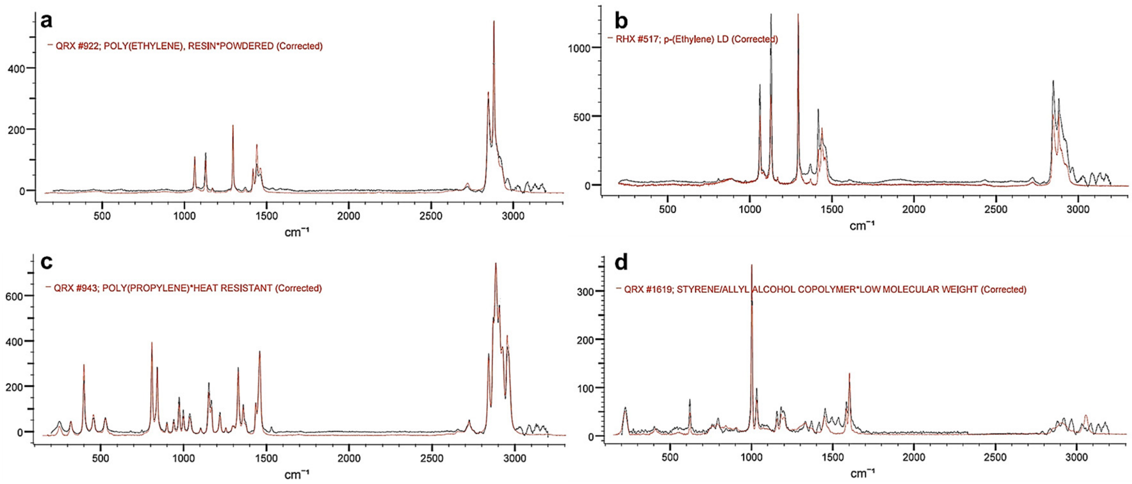

Figure 8. Raman spectra of polymers: (**a**,**b**) polyethylene; (**c**) polypropylene; and (**d**) polystyrene.

4. Discussions

By analyzing the predictions obtained from the tested models, we observed variations for each type of MP evaluated. The SVR model proved effective for pellets, although its performance was inferior to that of more robust models, such as RF and GB, used for other MP categories. References [64,75] emphasize that SVR is an efficient alternative for capturing patterns in less complex contexts, balancing simplicity and accuracy, especially in scenarios with low data non-linearity. In contrast, the RF model performed exceptionally well for foams because it handles complex interactions between variables and highly heterogeneous data. Reference [58] highlights that RF is ideal for contexts with many independent variables and/or high variability, making it particularly useful for predicting the deposition of lightweight and floating MPs, such as foams, which are influenced by wave energy and beach orientation [3,80].

The GB model was the most efficient for fragments, demonstrating its robustness in capturing non-linear relationships and its ability to handle complex and noisy data. References [61,71] note that GB is particularly effective in environmental scenarios with multiple interdependent factors. In this context, SHAP analysis revealed that morphometric variables, such as beach face slope and orientation, were key determinants for fragment deposition, reinforcing studies that emphasize the importance of morphometric variables in the dynamics of MPs in coastal zones [3,4,24].

In this context, the significant presence of pellets on beaches near the Port of Santos highlights the impact of industrial and port activities. These materials are frequently used as raw materials for producing plastic-derived items such as rigid packaging, pipes, and flexible containers. However, in these areas, these particles are prone to losses during transshipment and transportation, supporting studies that identify such locations as predominant sources of this type of microplastic [4,7,81,82]. The proximity to the port and industrial facilities is thus considered a significant factor contributing to the increased quantity of pellets on adjacent beaches such as PG, SVS, and GUA. Furthermore, Refs. [3,4,83] have shown that this specific type of MP tends to accumulate in the upper portions of the beach profile (storm surge strandlines), due to metoceanographic factors such as storm waves [84].

The VH, H, M, and VL concentrations of pellets associated with the modeled points on the beaches of PG, GUA, SVS, and BER indicate the influence of predominant longshore currents (NE-SW), which act as the primary force redistributing pellets southward along the São Paulo coastline [3,4,38,44,46,85,86]. Beaches downstream from the Port of Santos, such as PG, GUA, and SVS, are more heavily impacted, due to their proximity to pellet emission sources and the influence of the predominant currents, which redistribute these pollutants and cause their accumulation in these areas. Storm events intensify this process by moving pellets from the intertidal zones to the upper portions of the beach, particularly on those with faces oriented toward the southern quadrant [3,4,8,86,87].

In contrast, the modeled points located upstream and farther from these emission sources, such as BER, show a lower pellet accumulation [82]. However, pellets on these beaches may be related to their proximity to the Bertioga Channel, which connects directly to these sources (the Port of Santos and the Cubatão industrial complex). These areas are major distributors of such waste, especially during ebb tides, combined with the direct connection between the channel and the ocean, which facilitates the dispersion and deposition of these MPs on northern beaches, albeit on a smaller scale [3,8,46]. Additionally, SHAP analysis applied to predictive models reinforces that morphometric variables, such as beach slope and orientation, are key determinants for pellet deposition. South-facing intermediate beaches favor the accumulation of materials transported by longshore currents and extreme hydrodynamic events [3,4,38,75].

A previous analysis [3] observed that both beach face slope and Aspect showed significant associations and dependency relationships with all types of MP along the São Paulo coastline. The results presented here revealed that urban beaches, except for pellets, foams, fragments, and fibers, did not show significant associations with Aspect. Therefore, beach face orientation has a limited impact on the deposition of these other MP types. These MPs primarily originate from irregular in situ disposal by beachgoers and/or vendors, particularly in high-traffic beaches with inefficient cleaning during peak seasons (summer and holidays) [88–91], or through urban stormwater drainage systems that discharge onto these beaches. On a smaller scale, fishing gear waste transported by marine currents also contributes to these MPs. In contrast, pellets are deposited on beach profiles almost exclusively via the sea [3,82,90,92].

Pellets are predominantly composed of EPS and XPS, characterized by an extremely low density and high buoyancy [3,93–95]. These properties facilitate their transport by currents and waves, as well as their fragmentation due to UV radiation and mechanical abrasion, contributing to their dispersion and deposition in other coastal environments [23,88,96]. Foam deposition transported by the sea tends to accumulate in the lower and intermediate, more humid sections of the beach profile [3]. However, improperly discarded insulating packaging tends to break down into smaller particles through use, which accumulate in the upper sections of heavily frequented beaches, where wave energy is insufficient to remove these materials [97–99].

Poorly implemented beach cleaning exacerbates the issue. Urban beach cleaning often focuses on removing visible MPs while neglecting micro waste (<5 mm), which tends to remain in the upper sections of the beach. MPs also end up buried in the sand over time, similar to cigarette butts, requiring appropriate equipment to be removed [8,17]. In fact, even on Blue Flag-sealed beaches, although this certification represents an indication of beaches with higher environmental quality, this is not necessarily the reality. Reference [17] found that beaches that received this indication on the island of Cyprus (a tourist destination) and were cleaned once a day still presented this type of contaminant.

This oversight can worsen the presence of smaller pollutants, which not only persist in the environment for long periods, but also pose greater ecological and toxicological risks due to their interactions with marine organisms and their ability to adsorb chemical contaminants from the environment [24,28,29,82,100,101]. Due to their faceted or irregular shapes, fragments and fibers, commonly derived from packaging, household items, and industrial products, exhibit different transport and deposition dynamics on beaches compared to pellets and foams [9,24,101].

These geometric characteristics significantly increase resistance to movement, limiting their mobility and making it more difficult for them to be transported to the upper regions of beaches, particularly under less intense wind and wave conditions [102–104]. Unlike other types of MPs, such as pellets, fragments, and fibers are less likely to float or be displaced by lower-magnitude forces, which explains their higher concentration in the intermediate zones of the beach profile [3,5,24].

Another important factor is the density of fragments and fibers, which tends to be higher than that of lighter and more buoyant MPs, such as foams. This characteristic favors their deposition in areas where wave and current energy decreases but remains sufficient to mobilize them. In these zones, typically between the high tide line and areas with significant aeolian transport, fragments and fibers reach a dynamic equilibrium that hinders their movement to the upper sections of the beach [3].

Recent studies indicate that cleaning activities carried out by visitors at events created specifically for these purposes contribute not only to the removal of larger waste (litter), but also to valuing environmental education and a sense of belonging among participants when related to voluntary actions [105,106]. But, regarding MP residues, it is therefore evident that models combining remote sensing data with environmental variables (measured in situ) can assist in identifying and predicting zones of high MP accumulation [107], accounting for their type and addressing the high spatial complexity of these variables in coastal environments. Such models provide critical support for mitigation strategies [108–110] targeting this pollutant.

There is no doubt that, in general, beach pollution in Brazil is intensified by inadequate city waste management, which demonstrates that this problem requires a holistic approach [33] involving different stakeholders [111] and more effective public policies. Also, considering that the MPs found on beaches were not necessarily generated there, and that they may result from the fragmentation of larger pieces of plastic [23], the fight against beach pollution needs to be thought of in an interdisciplinary way, and by different levels of government, exposing its spatiotemporal complexity and borderless characteristics.

This study highlights the importance of using a large set of data to identify the hotspots where greater attention and monitoring [33] can maximize cleanup efforts and local solutions. As well as guiding mitigation measures and diplomatic efforts on the international level [112,113], reinforcing the urgency of a global legally binding treaty that is fair [113] and science-based [114,115] is critical to achieve target 14.1 proposed by the UN and other associated SDGs [111].

5. Conclusions

The study implemented rigorous protocols to ensure the reliability and reproducibility of the results. The calibration of ML models, evaluated through metrics such as R^2, MAE, RMSE, AIC, and BIC, mitigated overfitting and underfitting risks through careful data expansion and partitioning. SHAP analysis provided transparency by identifying the influence of individual variables. The polymer identifications, carried out using μ-Raman spectroscopy, incorporated noise filtering and iterative parameter adjustments for optimization. Together, these practices ensured data quality and model validity.

The results of this study highlighted the significant impact of MPs on urban beaches along the central São Paulo coastline, shedding light on their deposition dynamics and identifying the types of polymers present while exploring the relationship between these accumulations and environmental and morphometric factors. Applying techniques such as μ-Raman spectroscopy and ML models proved effective in characterizing MPs, indicating the primary sources of this pollutant (e.g., chemical industry, fishing activities, urban runoff, and local waste, etc.) and predicting their distributions. The predictive models emphasized the importance of variables such as beach slope (tanβ) and orientation (Aspect). Slope emerged as a critical variable influencing the deposition of all MP categories, while Aspect had a limited impact, being more relevant only for pellets. This finding suggests that on urban beaches, foams and other MP types (unlike pellets) are predominantly influenced by improper local solid waste disposal by beachgoers. This demonstrates that in these areas, the primary source of these other MP categories is not marine. In contrast, the deposition of pellets reflects a combination of marine transport and beach morphometric factors.

The research also highlights the variable performance of ML models in predicting different MP types, showcasing the unique characteristics of each material and its interactions with environmental factors. The study identified higher total MP concentrations in beaches south of the Port of Santos, such as PG, SVS, and GUA, attributed to their proximity to emission sources (beachgoers and urban stormwater drainage systems) and the influence of predominant NE-SW coastal drift currents. In contrast, northern beaches like BER exhibited lower total MP accumulation, though the hydrodynamic connection with the Bertioga Channel suggests a potential transport and deposition route for these areas.

Polymer characterization confirmed the predominance of polyethylene, polypropylene, and polystyrene, reflecting their industrial and disposable packaging origins. The study further underscores the need to improve waste management practices and the efficiency of urban beach cleanups, which often neglect smaller MPs. Incorporating these practices is essential to mitigate environmental and social impacts.

It is of great importance to contribute to tackling the challenges associated with MP pollution more efficiently and sustainably, in alignment with the SDGs, particularly SDG 14, which focuses on ocean conservation. By identifying land-based sources of pollution and predicting vulnerable marine areas, we provide essential data for preventive and remedial actions, supporting target 14.1 to reduce marine pollution by 2025. Furthermore, by supplying detailed information on the health of aquatic ecosystems, our findings assist in formulating sustainable management policies and implementing effective conservation strategies, helping to achieve target 14.2 of managing and protecting marine and coastal ecosystems. Finally, our research aims to advance scientific and technological knowledge in marine monitoring and conservation, promoting technology transfer and capacity building, which aligns with target 14.a to increase scientific knowledge and transfer marine technology.

Author Contributions: Conceptualization, A.T.d.S.F., R.C.d.O., E.S., M.C.H.R. and N.U.W.; methodology, A.T.d.S.F., R.C.d.O., E.S., M.C.H.R., L.S.E. and N.U.W.; validation, A.T.d.S.F., R.C.d.O., E.S., M.C.H.R. and N.U.W.; formal analysis, A.T.d.S.F., R.C.d.O., E.S., M.C.H.R., M.K., J.D., A.Z.d.F. and N.U.W.; investigation, A.T.d.S.F., R.C.d.O., E.S., M.C.H.R., M.K, J.D. and N.U.W.; resources, A.T.d.S.F., R.C.d.O., E.S. and N.U.W.; data curation, A.T.d.S.F., R.C.d.O., E.S. and N.U.W.; writing—original draft preparation, A.T.d.S.F., R.C.d.O., E.S., M.C.H.R., L.S.E., M.K., J.D., A.Z.d.F. and N.U.W.; writing—review and editing, A.T.d.S.F., R.C.d.O., E.S., M.C.H.R., L.S.E., M.K., J.D., A.Z.d.F. and N.U.W.; supervision, A.T.d.S.F., R.C.d.O., E.S., L.S.E. and N.U.W.; project administration, A.T.d.S.F.; funding acquisition, A.T.d.S.F., R.C.d.O., E.S. and N.U.W. All authors have read and agreed to the published version of the manuscript.

Funding: This study was funded by the São Paulo Research Foundation research fellows A.T.S.F. (FAPESP grant #2020/12050-6), N.U.W. (FAPESP grant #2021/-4334-7, and grant CNPq #3085262021-0), A.Z.F. (FAPESP grant #2018/19240-5, and CNPq-PQ #314079/2021-1), R.C.O. (grant CNPq #306931/2022-2), and E.S. (grant CNPq #308229/2022-3), who are National Council for Scientific and Technological Development (CNPq) research fellows. Acknowledgments are extended to the Editor-in-Chief, Associate Editor, and anonymous reviewers.

Institutional Review Board Statement: Not applicable.

Informed Consent Statement: Not applicable.

Data Availability Statement: Data table <https://doi.org/10.5281/zenodo.14248985>; Raman spectroscopy analysis <https://doi.org/10.5281/zenodo.14248963>.

Acknowledgments: The authors thank the Nuclear and Energy Research Institute, the Institute of Geosciences of the State University of Campinas, and the Oceanographic Institute of the University of São Paulo.

Conflicts of Interest: The authors declare no conflicts of interest.

References

1. Kershaw, P.J.; Turra, A.; Galgani, F. *GESAMP: Guidelines for the Monitoring and Assessment of Plastic Litter in the Ocean*; GESAMP: London, UK, 2019.
2. Löder, M.G.J.; Gerdts, G. Methodology Used for the Detection and Identification of Microplastics—A Critical Appraisal. In *BT—Marine Anthropogenic Litter*; Bergmann, M., Gutow, L., Klages, M., Eds.; Springer International Publishing: Cham, Switzerland, 2015; pp. 201–227, ISBN 978-3-319-16510-3.
3. Ferreira, A.T.d.S.; Wetter, N.U.; Ribeiro, M.C.H.; Esteves, L.S.; Dias, A.J.G.; Grohmann, C.H.; Kuznetsova, M.; Freitas, A.Z.d.; Oliveira, R.C.d.; Siegle, E. Recognizing Microplastic Deposits on Sandy Beaches by Altimetric Positioning, μ-Raman Spectroscopy and Multivariate Statistical Models. *Mar. Pollut. Bull.* **2024**, *209*, 117025. [CrossRef] [PubMed]
4. Ferreira, A.T.d.S.; Siegle, E.; Ribeiro, M.C.H.; Santos, M.S.T.; Grohmann, C.H. The Dynamics of Plastic Pellets on Sandy Beaches: A New Methodological Approach. *Mar. Environ. Res.* **2021**, *163*, 105219. [CrossRef] [PubMed]
5. Jambeck, J.R.; Ji, Q.; Zhang, Y.-G.; Liu, D.; Grossnickle, D.M.; Luo, Z.-X. Plastic Waste Inputs from Land into the Ocean. *Science (1979)* **2015**, *347*, 764–768. [CrossRef] [PubMed]
6. GESAMP. *Sources, Fate and Effects of Microplastics in the Marine Environment: A Global Assessment*; International Maritime Organization: London, UK, 2015.
7. Turra, A.; Manzano, A.B.; Dias, R.J.S.; Mahiques, M.M.; Barbosa, L.; Balthazar-Silva, D.; Moreira, F.T. Three-Dimensional Distribution of Plastic Pellets in Sandy Beaches: Shifting Paradigms. *Sci. Rep.* **2014**, *4*, 4435. [CrossRef]
8. Moreira, F.T.; Balthazar-Silva, D.; Barbosa, L.; Turra, A. Revealing Accumulation Zones of Plastic Pellets in Sandy Beaches. *Environ. Pollut.* **2016**, *218*, 313–321. [CrossRef]
9. Browne, M.A.; Galloway, T.S.; Thompson, R.C. Spatial Patterns of Plastic Debris along Estuarine Shorelines. *Environ. Sci. Technol.* **2010**, *44*, 3404–3409. [CrossRef]
10. Thompson, R.C.; Swan, S.H.; Moore, C.J.; Vom Saal, F.S. Our Plastic Age. *Philos. Trans. R. Soc. B Biol. Sci.* **2009**, *364*, 1973–1976. [CrossRef]
11. Parra, D.F.; Gimiliani, G.T.; Dos Santos, J.L.; Wetter, N.U.; Schepis, W.R.; Bereczki, A.; Cotrim, M.E.B. Microplastics in Santos São Vicente Estuarine–Hotspot in Sediments Caused by Low Energy Hydrodynamic Events in Strongly Populated Areas. *Mar. Pollut. Bull.* **2025**, *210*, 117286. [CrossRef]
12. Barnes, D.K.A.; Galgani, F.; Thompson, R.C.; Barlaz, M. Accumulation and Fragmentation of Plastic Debris in Global Environments. *Philos. Trans. R. Soc. B Biol. Sci.* **2009**, *364*, 1985–1998. [CrossRef] [PubMed]
13. Kaviarasan, T.; Dhineka, K.; Sambandam, M.; Sivadas, S.K.; Sivyer, D.; Hoehn, D.; Pradhan, U.; Mishra, P.; Murthy, M.V.R. Impact of Multiple Beach Activities on Litter and Microplastic Composition, Distribution, and Characterization along the Southeast Coast of India. *Ocean Coast. Manag.* **2022**, *223*, 106177. [CrossRef]
14. Stoica, E.; Nenciu, M.; Creangă, S.-M.; Tănase, M.-C.; Marin, D.; Ciucă, A.-M.; Pătrașcu, V. Assessment of the Marine Litter on the Romanian Black Sea Beaches. *Cercet. Mar. Rech. Mar.* **2021**, *51*, 49–63.
15. Wu, X.; Zhong, C.; Wang, T.; Zou, X.; Zang, Z.; Li, Q.; Chen, H. Occurrence and Distribution of Microplastics on Recreational Beaches of Haichow Bay, China. *Environ. Sci. Pollut. Res.* **2021**, *28*, 6132–6145. [CrossRef]
16. Mejía-Estrella, I.A.; Peña-Montes, C.; Peralta-Peláez, L.A.; Del Real Olvera, J.; Sulbarán-Rangel, B. Microplastics in Sandy Beaches of Puerto Vallarta in the Pacific Coast of Mexico. *Sustainability* **2023**, *15*, 15259. [CrossRef]
17. Loizidou, X.I.; Loizides, M.I.; Orthodoxou, D.L. Persistent Marine Litter: Small Plastics and Cigarette Butts Remain on Beaches after Organized Beach Cleanups. *Environ. Monit. Assess.* **2018**, *190*, 414. [CrossRef] [PubMed]
18. Kutralam-Muniasamy, G.; Pérez-Guevara, F.; Shruti, V.C. (Micro)Plastics: A Possible Criterion for Beach Certification with a Focus on the Blue Flag Award. *Sci. Total Environ.* **2022**, *803*, 150051. [CrossRef] [PubMed]
19. Borriello, A. Preferences for Microplastic Marine Pollution Management Strategies: An Analysis of Barriers and Enablers for More Sustainable Choices. *J. Environ. Manag.* **2023**, *344*, 118382. [CrossRef]

20. Corbau, C.; Lazarou, A.; Buoninsegni, J.; Olivo, E.; Gazale, V.; Nardin, W.; Simeoni, U.; Carboni, D. Linking Marine Litter Accumulation and Beach User Perceptions on Pocket Beaches of Northern Sardinia (Italy). *Ocean Coast. Manag.* **2023**, *232*, 106442. [CrossRef]
21. Ghosh, S.; Sinha, J.K.; Ghosh, S.; Vashisth, K.; Han, S.; Bhaskar, R. Microplastics as an Emerging Threat to the Global Environment and Human Health. *Sustainability* **2023**, *15*, 10821. [CrossRef]
22. Wyles, K.J.; Pahl, S.; Thomas, K.; Thompson, R.C. Factors That Can Undermine the Psychological Benefits of Coastal Environments: Exploring the Effect of Tidal State, Presence, and Type of Litter. *Environ. Behav.* **2016**, *48*, 1095–1126. [CrossRef]
23. Harris, P.T. The Fate of Microplastic in Marine Sedimentary Environments: A Review and Synthesis. *Mar. Pollut. Bull.* **2020**, *158*, 111398. [CrossRef]
24. Andrady, A.L. Microplastics in the Marine Environment. *Mar. Pollut. Bull.* **2011**, *62*, 1596–1605. [CrossRef]
25. Royer, S.-J.; Ferrón, S.; Wilson, S.T.; Karl, D.M. Production of Methane and Ethylene from Plastic in the Environment. *PLoS ONE* **2018**, *13*, e0200574. [CrossRef] [PubMed]
26. Van Cauwenberghe, L.; Devriese, L.; Galgani, F.; Robbens, J.; Janssen, C.R. Microplastics in Sediments: A Review of Techniques, Occurrence and Effects. *Mar. Environ. Res.* **2015**, *111*, 5–17. [CrossRef] [PubMed]
27. Choy, C.A.; Robison, B.H.; Gagne, T.O.; Erwin, B.; Firl, E.; Halden, R.U.; Hamilton, J.A.; Katija, K.; Lisin, S.E.; Rolsky, C.; et al. The Vertical Distribution and Biological Transport of Marine Microplastics across the Epipelagic and Mesopelagic Water Column. *Sci. Rep.* **2019**, *9*, 7843. [CrossRef] [PubMed]
28. Fisner, M.; Taniguchi, S.; Moreira, F.; Bícego, M.C.; Turra, A. Polycyclic Aromatic Hydrocarbons (PAHs) in Plastic Pellets: Variability in the Concentration and Composition at Different Sediment Depths in a Sandy Beach. *Mar. Pollut. Bull.* **2013**, *70*, 219–226. [CrossRef]
29. Fisner, M.; Majer, A.; Taniguchi, S.; Bícego, M.; Turra, A.; Gorman, D. Colour Spectrum and Resin-Type Determine the Concentration and Composition of Polycyclic Aromatic Hydrocarbons (PAHs) in Plastic Pellets. *Mar. Pollut. Bull.* **2017**, *122*, 323–330. [CrossRef]
30. Fisner, M.; Taniguchi, S.; Majer, A.P.; Bícego, M.C.; Turra, A. Concentration and Composition of Polycyclic Aromatic Hydrocarbons (PAHs) in Plastic Pellets: Implications for Small-Scale Diagnostic and Environmental Monitoring. *Mar. Pollut. Bull.* **2013**, *76*, 349–354. [CrossRef]
31. Escrobot, M.; Pagioro, T.A.; Martins, L.R.R.; de Freitas, A.M. Microplastics in Brazilian Coastal Environments: A Systematic Review. *Rev. Bras. Ciências Ambient. (RBCIAMB)* **2024**, *59*, e1719. [CrossRef]
32. Ferreira, A.T.d.S.; Oliveira, R.C.d.; Ribeiro, M.C.H.; Grohmann, C.H.; Siegle, E. Coastal Dynamics Analysis Based on Orbital Remote Sensing Big Data and Multivariate Statistical Models. *Coasts* **2023**, *3*, 160–174. [CrossRef]
33. Alencar, M.V.; Gimenez, B.G.; Sasahara, C.; Elliff, C.I.; Velis, C.A.; Rodrigues, L.S.; Conti, L.A.; Gonçalves-Dias, S.L.F.; Cetrulo, T.B.; Scrich, V.M.; et al. Advancing Plastic Pollution Hotspotting at the Subnational Level: Brazil as a Case Study in the Global South. *Mar. Pollut. Bull.* **2023**, *194*, 115382. [CrossRef]
34. Kida, M.; Pochwat, K.; Ziembowicz, S. Assessment of Machine Learning-Based Methods Predictive Suitability for Migration Pollutants from Microplastics Degradation. *J. Hazard. Mater.* **2024**, *461*, 132565. [CrossRef]
35. Zhen, Y.; Wang, L.; Sun, H.; Liu, C. Prediction of Microplastic Abundance in Surface Water of the Ocean and Influencing Factors Based on Ensemble Learning. *Environ. Pollut.* **2023**, *331*, 121834. [CrossRef]
36. Cai, C.; Zhu, L.; Hong, B. A Review of Methods for Modeling Microplastic Transport in the Marine Environments. *Mar. Pollut. Bull.* **2023**, *193*, 115136. [CrossRef]
37. Lin, J.; Liu, H.; Zhang, J. Recent Advances in the Application of Machine Learning Methods to Improve Identification of the Microplastics in Environment. *Chemosphere* **2022**, *307*, 136092. [CrossRef]
38. Ferreira, A.T.d.S.; de Oliveira, R.C.; Ribeiro, M.C.H.; de Freitas Sousa, P.S.; de Paula Miranda, L.; de Oliveira Folharini, S.; Siegle, E. Microplastic Deposit Predictions on Sandy Beaches by Geotechnologies and Machine Learning Models. *Coasts* **2025**, *5*, 4. [CrossRef]
39. Bereczki, A.; Dipold, J.; Freitas, A.Z.; Wetter, N.U. Sub-10 Nm Nanoparticle Detection Using Multi-Technique-Based Micro-Raman Spectroscopy. *Polymers* **2023**, *15*, 4644. [CrossRef]
40. Li, J.; Liu, H.; Chen, J.P. Microplastics in Freshwater Systems: A Review on Occurrence, Environmental Effects, and Methods for Microplastics Detection. *Water Res.* **2018**, *137*, 362–374. [CrossRef]
41. dos Santos, J.L.; Bereczki, A.; Pascoal, D.R.d.C.; Gimiliani, G.T.; Cotrim, M.E.B.; de Freitas, A.Z.; Wetter, N.U.; Parra, D.F. Combination of Micro-Raman and Infrared Spectroscopy to Identify Intriguing Case of Aged Microplastics of Estuarine Sediments. *Macromol. Symp.* **2024**, *413*, 1. [CrossRef]
42. Sebastião, G.I.A.; Rani-Borges, B.; Dipold, J.; Freitas, A.Z.; Wetter, N.U.; Ando, R.A.; Waldman, W.R. Forensic Determination of Adhesive Vinyl Microplastics in Urban Soils. *J. Environ. Manag.* **2025**, *373*, 123498. [CrossRef]
43. *United Nations Resolution Adopted by the General Assembly on 11 September 2015*; New York United Nations: New York, NY, USA, 2015.

44. Tessler, M.; Goya, S.; Yoshikawa, P.H.S. Erosão e Progradação Do Litoral Brasileiro–São Paulo. In *Erosão e Progradação no Litoral Brasileiro. Dieter Muehe (org.), Brasília, MMA*; Muehe, D., Ed.; MMA: Brasília, Brasil, 2018; pp. 297–346.
45. Andrade, T.S.d; Sousa, P.H.G.d.O.; Siegle, E. Vulnerability to Beach Erosion Based on a Coastal Processes Approach. *Appl. Geogr.* **2019**, *102*, 12–19. [CrossRef]
46. Harari, J.; Camargo, R. de Modelagem Numérica Da Região Costeira de Santos (SP): Circulação de Maré. *Rev. Bras. Oceanogr.* **1998**, *46*, 135–156. [CrossRef]
47. Pianca, C.; Mazzini, P.L.F.; Siegle, E. Brazilian Offshore Wave Climate Based on NWW3 Reanalysis. *Braz. J. Oceanogr.* **2010**, *58*, 53–70. [CrossRef]
48. Corrêa, M.R.; Xavier, L.Y.; Gonçalves, L.R.; Andrade, M.M.d.; Oliveira, M.d.; Malinconico, N.; Botero, C.M.; Milanés, C.; Montero, O.P.; Defeo, O. Desafios Para Promoção Da Abordagem Ecossistêmica à Gestão de Praias Na América Latina e Caribe. *Estud. Avançados* **2021**, *35*, 219–236. [CrossRef]
49. Franzen, M.O.; Fernandes, E.H.L.; Siegle, E. Impacts of Coastal Structures on Hydro-Morphodynamic Patterns and Guidelines towards Sustainable Coastal Development: A Case Studies Review. *Reg. Stud. Mar. Sci.* **2021**, *44*, 101800. [CrossRef]
50. Burrough, P.A.; McDonnell, R.A.; Lloyd, C.D. *Principles of Geographical Information Systems*; Oxford University Press: New York, NY, USA, 2015; ISBN 0198742843.
51. DHN. *F—41-Descrição de Estação Maregráfica*; Praticagem: Santos, Brazil, 2017.
52. Parreiras, T.C.; Bolfe, E.L.; Sano, E.S.; Victoria, D.d.C.; Sanches, I.D.; Vicente, L.E. Exploring the Harmonized Landsat Sentinel (Hls) Datacube to Map AN Agricultural Landscape in the Brazilian Savanna. *Int. Arch. Photogramm. Remote Sens. Spat. Inf. Sci.* **2022**, *43*, 967–973. [CrossRef]
53. Flater, D. WXTide32. Available online: http://www.wxtide32.com/index.html (accessed on 21 January 2025).
54. Bujan, N.; Cox, R.; Masselink, G. From Fine Sand to Boulders: Examining the Relationship between Beach-Face Slope and Sediment Size. *Mar. Geol.* **2019**, *417*, 106012. [CrossRef]
55. Vos, K.; Harley, M.D.; Splinter, K.D.; Walker, A.; Turner, I.L. Beach Slopes from Satellite-Derived Shorelines. *Geophys. Res. Lett.* **2020**, *47*, e2020GL088365. [CrossRef]
56. Blitzkow, D.; de Matos, A.C.O.C.; Xavier, E.M.L.; Fortes, L.P.S. MAPGEO2015: O Novo Modelo de Ondulação Geoidal Do Brasil. *Rev. Bras. Cartogr.* **2016**, *68*, 1873–1884. [CrossRef]
57. Ferreira, A.T.S.; Grohmann, C.H.; Ribeiro, M.C.H.; Santos, M.S.T.; de Oliveira, R.C.; Siegle, E. Beach Surface Model Construction: A Strategy Approach with Structure from Motion-Multi-View Stereo. *MethodsX* **2024**, *12*, 102694. [CrossRef] [PubMed]
58. McCreery, R.L. *Raman Spectroscopy for Chemical Analysis*; John Wiley & Sons: Hoboken, NJ, USA, 2005; ISBN 0471231878.
59. Ferraro, J.R. *Introductory Raman Spectroscopy*; Elsevier: Amsterdam, The Netherlands, 2003; ISBN 0080509126.
60. Smith, E.; Dent, G. *Modern Raman Spectroscopy: A Practical Approach*; John Wiley & Sons: Hoboken, NJ, USA, 2019; ISBN 1119440556.
61. Araujo, C.F.; Nolasco, M.M.; Ribeiro, A.M.P.; Ribeiro-Claro, P.J.A. Identification of Microplastics Using Raman Spectroscopy: Latest Developments and Future Prospects. *Water Res.* **2018**, *142*, 426–440. [CrossRef]
62. Breiman, L. Random Forests. *Mach. Learn.* **2001**, *45*, 5–32. [CrossRef]
63. Fávero, L.P.; Belfiore, P. *Manual de Análise de Dados: Estatística e Modelagem Multivariada Com Excel®, SPSS® e Stata®*; Elsevier: Rio de Janeiro, Brasil, 2017.
64. Kohavi, R. *A Study of Cross-Validation and Bootstrap for Accuracy Estimation and Model Selection*; Morgan Kaufman Publishing: Burlington, MA, USA, 1995.
65. Friedman, J.H. Greedy Function Approximation: A Gradient Boosting Machine. *Ann. Stat.* **2001**, *29*, 1189–1232. [CrossRef]
66. Hoerl, A.E.; Kennard, R.W. Ridge Regression: Biased Estimation for Nonorthogonal Problems. *Technometrics* **1970**, *12*, 55–67. [CrossRef]
67. Tibshirani, R. Regression Shrinkage and Selection via the Lasso. *J. R. Stat. Soc. Ser. B Stat. Methodol.* **1996**, *58*, 267–288. [CrossRef]
68. Smola, A.J.; Schölkopf, B. A Tutorial on Support Vector Regression. *Stat. Comput.* **2004**, *14*, 199–222. [CrossRef]
69. Vapnik, V. *The Nature of Statistical Learning Theory*; Springer Science & Business Media: Berlin/Heidelberg, Germany, 2013; ISBN 1475732643.
70. Wold, S.; Sjöström, M.; Eriksson, L. PLS-Regression: A Basic Tool of Chemometrics. *Chemom. Intell. Lab. Syst.* **2001**, *58*, 109–130. [CrossRef]
71. Géron, A. *Hands-on Machine Learning with Scikit-Learn, Keras, and TensorFlow*; O' Reilly Media, Inc.: Sebastopo, CA, USA, 2022; ISBN 1098122461.
72. Hastie, T.; Tibshirani, R.; Friedman, J.H.; Friedman, J.H. *The Elements of Statistical Learning: Data Mining, Inference, and Prediction*; Springer: Berlin/Heidelberg, Germany, 2009; Volume 2.
73. Willmott, C.J.; Ackleson, S.G.; Davis, R.E.; Feddema, J.J.; Klink, K.M.; Legates, D.R.; O'donnell, J.; Rowe, C.M. Statistics for the Evaluation and Comparison of Models. *J. Geophys. Res. Ocean.* **1985**, *90*, 8995–9005. [CrossRef]
74. Schwarz, G. Estimating the Dimension of a Model. *Ann. Stat.* **1978**, *6*, 461–464. [CrossRef]
75. Lundberg, S. A Unified Approach to Interpreting Model Predictions. *arXiv* **2017**, arXiv:1705.07874.

76. Haberman, S.J. *Analysis of Qualitative Data: Introductory Topics*; Academic Press, Incorporated: New York, NY, USA, 1978.
77. Johnson, R.A.; Wichern, D.W. *Applied Multivariate Statistical Analysis*; Springer: Berlin/Heidelberg, Germany, 1992; Volume 405.
78. Souto, L.D.S.; Souto, E. *de S. Análise de Dados Ecológicos*, 1st ed.; Clude de Autores: Brasília, Brazil, 2020; ISBN 9788591080526.
79. Das, S.; Roy Maulik, S. Recent Approaches and Advancements in Natural Dyes. *Nat. Dye. Sustain.* **2024**, 63–78. [CrossRef]
80. Zeng, E.Y. *Microplastic Contamination in Aquatic Environments: An Emerging Matter of Environmental Urgency*; Elsevier: Amsterdam, The Netherlands, 2023; ISBN 0443153337.
81. Balthazar-Silva, D.; Turra, A.; Moreira, F.T.; Camargo, R.M.; Oliveira, A.L.; Barbosa, L.; Gorman, D. Rainfall and Tidal Cycle Regulate Seasonal Inputs of Microplastic Pellets to Sandy Beaches. *Front. Environ. Sci.* **2020**, *8*, 123. [CrossRef]
82. Izar, G.M.; Morais, L.G.; Pereira, C.D.S.; Cesar, A.; Abessa, D.M.S.; Christofoletti, R.A. Quantitative Analysis of Pellets on Beaches of the São Paulo Coast and Associated Non-Ingested Ecotoxicological Effects on Marine Organisms. *Reg. Stud. Mar. Sci.* **2019**, *29*, 100705. [CrossRef]
83. Alvarez-Zeferino, J.C.; Ojeda-Benítez, S.; Cruz-Salas, A.A.; Martínez-Salvador, C.; Vázquez Morillas, A. Dataset of Quantification and Classification of Microplastics in Mexican Sandy Beaches. *Data Brief* **2020**, *33*, 106473. [CrossRef]
84. Furlan, I.; Fornari, M.; Sawakuchi, A.O.; Giannini, P.C.F.; Dipold, J.; de Freitas, A.Z.; Wetter, N.U.; Semensatto, D. Morphodynamics Drive the Transport and Accumulation of Anthropogenic Microparticles in Tropical Coastal Depositional Systems in Southeastern Brazil. *Sci. Total Environ.* **2024**, *957*, 177479. [CrossRef]
85. Goya, S.C.Y.; Tessler, M.G. Erosão Costeira: Exemplos No Litoral Brasileiro. In *Gestão de Praias: Do Conceito à Prática*; Instituto de Estudos Avançados da Universidade de São Paulo: São Paulo, Brazil, 2022; pp. 65–89.
86. Camargo, R.d.; Harari, J. Modelagem Numérica de Ressacas Na Plataforma Sudeste Do Brasil a Partir de Cartas Sinóticas de Pressão Atmosférica Na Superfície. *Bol. Inst. Ocean.* **1994**, *42*, 19–34. [CrossRef]
87. Kukulka, T.; Proskurowski, G.; Morét-Ferguson, S.; Meyer, D.W.; Law, K.L. The Effect of Wind Mixing on the Vertical Distribution of Buoyant Plastic Debris. *Geophys. Res. Lett.* **2012**, *39*, 7601. [CrossRef]
88. Chen, S.; Lin, D.; Gao, G.; Guan, J.; Belver, C.; Bedia, J. Sources, Aging, and Management of Coastal Plastics in Shanghai. *Water Air Soil Pollut.* **2022**, *233*, 437. [CrossRef]
89. Zamora, A.M.; da Gama, B.A.P.; de Oliveira, J.D.N.; Soares-Gomes, A. Cleaning Efficiency in a Southwestern Atlantic Sandy Beach. *Reg. Stud. Mar. Sci.* **2021**, *45*, 101865. [CrossRef]
90. da Silva, E.F.; do Carmo, D.d.F.; Muniz, M.C.; Dos Santos, C.A.; Cardozo, B.B.I.; de Oliveira Costa, D.M.; Dos Anjos, R.M.; Vezzone, M. Evaluation of Microplastic and Marine Debris on the Beaches of Niterói Oceanic Region, Rio De Janeiro, Brazil. *Mar. Pollut. Bull.* **2022**, *175*, 113161. [CrossRef]
91. da Silva, M.L.; Castro, R.O.; Sales, A.S.; de Araújo, F.V. Marine Debris on Beaches of Arraial Do Cabo, RJ, Brazil: An Important Coastal Tourist Destination. *Mar. Pollut. Bull.* **2018**, *130*, 153–158. [CrossRef]
92. da Silva, M.L.; de Araújo, F.V.; Castro, R.O.; Sales, A.S. Spatial–Temporal Analysis of Marine Debris on Beaches of Niterói, RJ, Brazil: Itaipu and Itacoatiara. *Mar. Pollut. Bull.* **2015**, *92*, 233–236. [CrossRef] [PubMed]
93. Turner, A. Foamed Polystyrene in the Marine Environment: Sources, Additives, Transport, Behavior, and Impacts. *Environ. Sci. Technol.* **2020**, *54*, 10411–10420. [CrossRef] [PubMed]
94. Auta, H.S.; Emenike, C.U.; Fauziah, S.H. Distribution and Importance of Microplastics in the Marine Environment: A Review of the Sources, Fate, Effects, and Potential Solutions. *Environ. Int.* **2017**, *102*, 165–176. [CrossRef]
95. Gao, G.H.Y.; Helm, P.; Baker, S.; Rochman, C.M. Bromine Content Differentiates between Construction and Packaging Foams as Sources of Plastic and Microplastic Pollution. *ACS ES&T Water* **2023**, *3*, 876–884.
96. Costa, L.L.; Fanini, L.; Ben-Haddad, M.; Pinna, M.; Zalmon, I.R. Marine Litter Impact on Sandy Beach Fauna: A Review to Obtain an Indication of Where Research Should Contribute More. *Microplastics* **2022**, *1*, 554–571. [CrossRef]
97. Robbe, E.; Woelfel, J.; Balčiūnas, A.; Schernewski, G. An Impact Assessment of Beach Wrack and Litter on Beach Ecosystem Services to Support Coastal Management at the Baltic Sea. *Environ. Manag.* **2021**, *68*, 835–859. [CrossRef]
98. Ziani, K.; Ioniță-Mîndrican, C.-B.; Mititelu, M.; Neacșu, S.M.; Negrei, C.; Moroșan, E.; Drăgănescu, D.; Preda, O.-T. Microplastics: A Real Global Threat for Environment and Food Safety: A State of the Art Review. *Nutrients* **2023**, *15*, 617. [CrossRef]
99. Zielinski, S.; Botero, C.M.; Yanes, A. To Clean or Not to Clean? A Critical Review of Beach Cleaning Methods and Impacts. *Mar. Pollut. Bull.* **2019**, *139*, 390–401. [CrossRef]
100. Browne, M.A.; Crump, P.; Niven, S.J.; Teuten, E.; Tonkin, A.; Galloway, T.; Thompson, R. Accumulation of Microplastic on Shorelines Woldwide: Sources and Sinks. *Environ. Sci. Technol.* **2011**, *45*, 9175–9179. [CrossRef]
101. Cole, M.; Lindeque, P.; Halsband, C.; Galloway, T.S. Microplastics as Contaminants in the Marine Environment: A Review. *Mar. Pollut. Bull.* **2011**, *62*, 2588–2597. [CrossRef]
102. de Oliveira, C.R.S.; da Silva Júnior, A.H.; Mulinari, J.; Ferreira, A.J.S.; da Silva, A. Fibrous Microplastics Released from Textiles: Occurrence, Fate, and Remediation Strategies. *J. Contam. Hydrol.* **2023**, *256*, 104169. [CrossRef] [PubMed]

103. Lefebvre, C.; Le Bihanic, F.; Jalón-Rojas, I.; Dusacre, E.; Chassaigne, L.; Bichon, J.; Clérandeau, C.; Morin, B.; Lecomte, S.; Cachot, J. Spatial Distribution of Anthropogenic Particles and Microplastics in a Meso-Tidal Lagoon (Arcachon Bay, France): A Multi-Compartment Approach. *Sci. Total Environ.* **2023**, *898*, 165460. [CrossRef]
104. Zhang, C.; Wang, Q.; Zhao, J.M.; Zhao, Y.J.; Shan, E.C. Observational and Model Studies on Transport and Inventory of Microplastics from a Leak Accident on the Beaches of Yantai. *Mar. Pollut. Bull.* **2022**, *182*, 113976. [CrossRef] [PubMed]
105. Wyles, K.J.; Pahl, S.; Holland, M.; Thompson, R.C. Can Beach Cleans Do More than Clean-up Litter? Comparing Beach Cleans to Other Coastal Activities. *Environ. Behav.* **2017**, *49*, 509–535. [CrossRef]
106. Rayon-Viña, F.; Miralles, L.; Fernandez-Rodríguez, S.; Dopico, E.; Garcia-Vazquez, E. Marine Litter and Public Involvement in Beach Cleaning: Disentangling Perception and Awareness among Adults and Children, Bay of Biscay, Spain. *Mar. Pollut. Bull.* **2019**, *141*, 112–118. [CrossRef]
107. Hong, P.; Xiao, J.; Liu, H.; Niu, Z.; Ma, Y.; Wang, Q.; Zhang, D.; Ma, Y. An Inversion Model of Microplastics Abundance Based on Satellite Remote Sensing: A Case Study in the Bohai Sea. *Sci. Total Environ.* **2024**, *909*, 168537. [CrossRef]
108. Khriss, A.; Elmiad, K.A.; Badaoui, M.; Barkaoui, A.; Zarhloule, Y. Advances in Machine Learning and Deep Learning Approaches for Plastic Litter Detection in Marine Environments. *J. Theor. Appl. Inf. Technol.* **2024**, *102*, 1885.
109. Su, J.; Zhang, F.; Yu, C.; Zhang, Y.; Wang, J.; Wang, C.; Wang, H.; Jiang, H. Machine Learning: Next Promising Trend for Microplastics Study. *J. Environ. Manag.* **2023**, *344*, 118756. [CrossRef] [PubMed]
110. Chaczko, Z.; Wajs-Chaczko, P.; Tien, D.; Haidar, Y. Detection of Microplastics Using Machine Learning. In Proceedings of the 2019 International Conference on Machine Learning and Cybernetics (ICMLC), Kobe, Japan, 7–10 July 2019; IEEE: Piscataway, NJ, USA, 2019; pp. 1–8.
111. Stoett, P.; Scrich, V.M.; Elliff, C.I.; Andrade, M.M.; Grilli, N.d.M.; Turra, A. Global Plastic Pollution, Sustainable Development, and Plastic Justice. *World Dev.* **2024**, *184*, 106756. [CrossRef]
112. Polejack, A. The Importance of Ocean Science Diplomacy for Ocean Affairs, Global Sustainability, and the UN Decade of Ocean Science. *Front. Mar. Sci.* **2021**, *8*, 248. [CrossRef]
113. Dauvergne, P. The Necessity of Justice for a Fair, Legitimate, and Effective Treaty on Plastic Pollution. *Mar. Policy* **2023**, *155*, 105785. [CrossRef]
114. Aanesen, M.; Ahi, J.C.; Abate, T.G.; Khan, F.R.; de Vries, F.P.; Kite-Powell, H.; Beaumont, N.J. Insights from International Environmental Legislation and Protocols for the Global Plastic Treaty. *Sci. Rep.* **2024**, *14*, 2750. [CrossRef] [PubMed]
115. Brander, S.M.; Senathirajah, K.; Fernandez, M.O.; Weis, J.S.; Kumar, E.; Jahnke, A.; Hartmann, N.B.; Alava, J.J.; Farrelly, T.; Almroth, B.C. The Time for Ambitious Action Is Now: Science-Based Recommendations for Plastic Chemicals to Inform an Effective Global Plastic Treaty. *Sci. Total Environ.* **2024**, *949*, 174881. [CrossRef] [PubMed]